Long-Term Trend in Fabry-Perot Interferometer Observations of Thermospheric F-Region Neutral Temperatures Based on Doppler Widths of the 630 nm Oxygen Emission

Rajan Itani, Mark Conde

Geophysical Institute, University of Alaska Fairbanks

Introduction and Overview:

We have examined the long-term trend in 630 nm Doppler temperatures of the F-region thermosphere at high latitudes. Consistent with previous studies, we found a cooling trend of -27.4±6.2 K/decade.

The emission of greenhouse gases is believed to be causing atmospheric warming at the Earth's surface. By contrast, various theoretical and model studies suggest that greenhouse gas build-up should lead to a decrease in thermospheric temperature [e.g., Roble and Dickinson (1989)]. Further, incoherent scatter radar (ISR) studies show cooling trends of approximately -20 K/decade at an altitude of 250 km (Donaldson et al., 2010) and -12 K/decade at an altitude of 250-300 km (Zhang et al., 2011). As the atmosphere cools the mass density at a given height decreases. This not only increases the orbital lifetime of low Earth orbit satellites but also slows the removal of space debris from this region. Previous studies also suggested that the relative change in temperature in the thermosphere as a result of climate change is larger than that near the Earth's surface. Any climatological trend would thus be expected to be apparent sooner in the upper atmosphere. The upper atmosphere can thus be used as an early warning system. Results of long-term trend studies can also be used in planning future satellite missions.

Instruments and Methods:

Upper atmospheric temperatures can be measured in situ by satellites or rockets, or else by remote sensing. In this work, we made ground-based observations of thermospheric temperature using Fabry-Perot interferometers (FPIs) to measure the Doppler width of the 630 nm optical emission from atomic oxygen. The particular type of FPIs used in this work are known as Scanning Doppler Imagers (SDIs). SDIs are FPIs capable of simultaneously viewing a zenith-centered circular field of view (FoV) in the sky spanning roughly 150^0 full angle. The FoV was typically subdivided into 115 independent zones. Spectral sampling for each zone was obtained by scanning the etalon gap over one order of interference. The instrument and the spectral fitting techniques are explained in detail by Conde and Smith (1995, 1997, 1998).

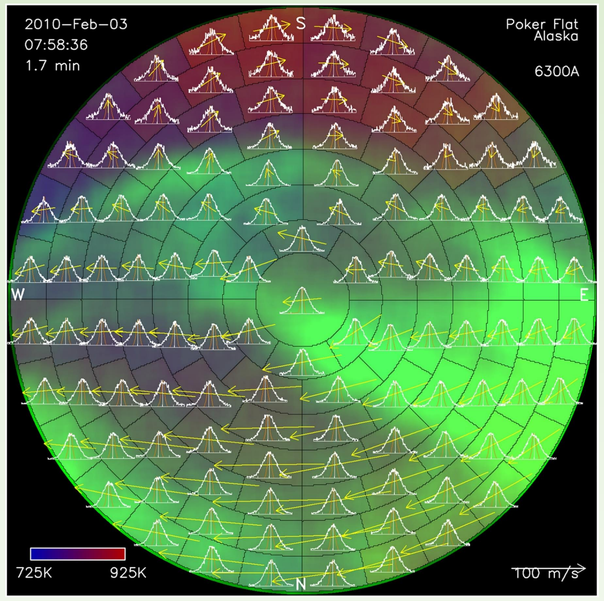

Figure 1. SDI's zenith-centered FOV divided into 115 zones. White curves show spectra acquired from each zone. Blue through red colors depict the temperatures derived from the spectrum from each zone. Green hues depict 630 nm emission intensity. Yellow arrows indicate the fitted horizontal wind field. (Conde et al., 2018)

Data:

F-region neutral temperature measurements were compiled from eight different sites - five in Alaska, and three in Antarctica. Data were available from the years 1995 to 2021. All measurements were quality controlled based on the chi-squared parameter of the spectral fit, signal-to-noise ratio of the spectra, and possible signatures of cloudiness in the data. Total numbers of observations for each year from 1995 to 2021 are shown in Table-1.

Year	Raw Data	Median Data	Year	Raw Data	Median Data
1995	1471	90	2009	1408281	13224
1996	1435	48	2010	2819889	25514
1997	19210	968	2011	5607282	47558
1998	44754	1969	2012	9361364	83702
1999	113788	4618	2013	10597562	94222
2000	260565	6866	2014	7675279	68366
2001	534786	12174	2015	5212486	46324
2002	335115	7436	2016	23842621	171924
2003	27619	439	2017	8717180	76859
2004	14978	325	2018	8898940	80078
2005	1911	15	2019	6085461	55003
2007	417154	7085	2020	4429829	39717
2008	1960420	21147	2021	1859714	16414
		Total Raw Data	100249094		
		Total Median Data	882085		

Table 1. Total number of temperature observations from individual zones from each year and the number of all-sky median observations in each year.

Possible Instrumental Effects:

Spectra recorded by SDI instruments include instrumental broadening which can be approximated as:

$$\sigma_{obs}^2 = \sigma_{sky}^2 + \sigma_{ins}^2$$

where, σ_{obs} = Line width of observed spectra

σ_{sky} = Line width of sky spectra

σ_{ins} = Instrument function

This broadening is explicitly accounted for while deriving temperatures. However, the SDI instruments have evolved over time; newer instruments have narrower passbands - as illustrated in Figure 2. We must therefore establish whether the origin of any long-term trend in our climatological average temperature data is instrumental or geophysical. (i.e., imperfect removal of instrumental broadening could potentially produce an erroneous apparent long-term trend in thermospheric temperature.) Artifacts, if any, for older instruments with broader instrument functions would be expected to appear as erroneously low inferred temperatures. In contrast, for newer instruments with narrower passbands an imperfect accounting of instrumental broadening would produce higher inferred temperatures. These scenarios are opposite of the observed trend shown in panel c of Figure 4 indicating the trend to be of geophysical origin rather than an instrumental artifact.

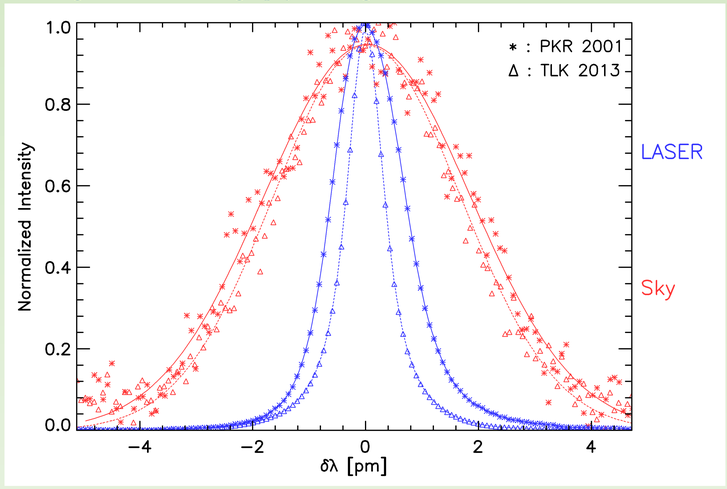

Figure 2. Sky and laser spectra of the 630 nm emission line for the zenith FoV zones recorded on 17 January 2013 from Toolik Lake and 23 November 2001 from Poker Flat, Alaska, as indicated by the plot symbols. Red data points denote the observed sky spectra, and red solid curves are fitted versions of the observed spectra. Blue color represents the same for laser spectra. The Toolik Lake sky spectrum was generated by two scans of etalon for an exposure time of 32 seconds and that from Poker Flat was generated by 26 scans of etalon for a total exposure time of 369 seconds. SDIs automatically adjust the exposure times based on airglow/auroral intensity to achieve a predefined signal-to-noise ratio.

Results:

SDI Temperatures vs MSIS model Temperatures:

Effects of various sources of temperature variability like solar activity, geomagnetic activity, season, and time of day in the observed temperatures should be accounted for in order to analyze the trend. For this, we have used the NRLMSISE-00 (hereinafter referred to as MSIS) model temperatures as shown in Figure 3, which shows a strong correlation between the observed and model temperatures. We corrected for geophysical variability by subtracting from our data the corresponding predicted MSIS temperatures. Because the MSIS model coefficients are constant with time, any long-term trend in the observation minus MSIS difference is presumably due to long-term climatological changes in the observations.

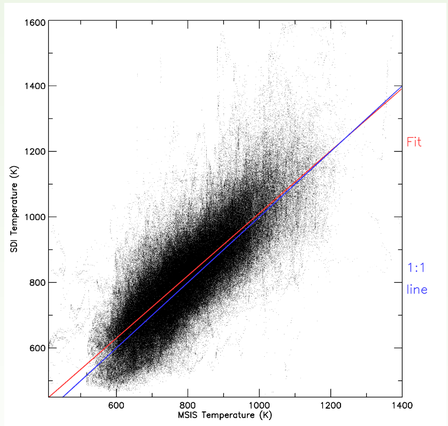

Figure 3. Median SDI temperatures for all stations for all years plotted as a function of the corresponding predicted MSIS model temperatures. MSIS model temperatures were calculated using the appropriate geophysical values that correspond to the observations. The blue and the red solid lines show a unit slope line and a linear fit to the data respectively.

Temperature Trend:

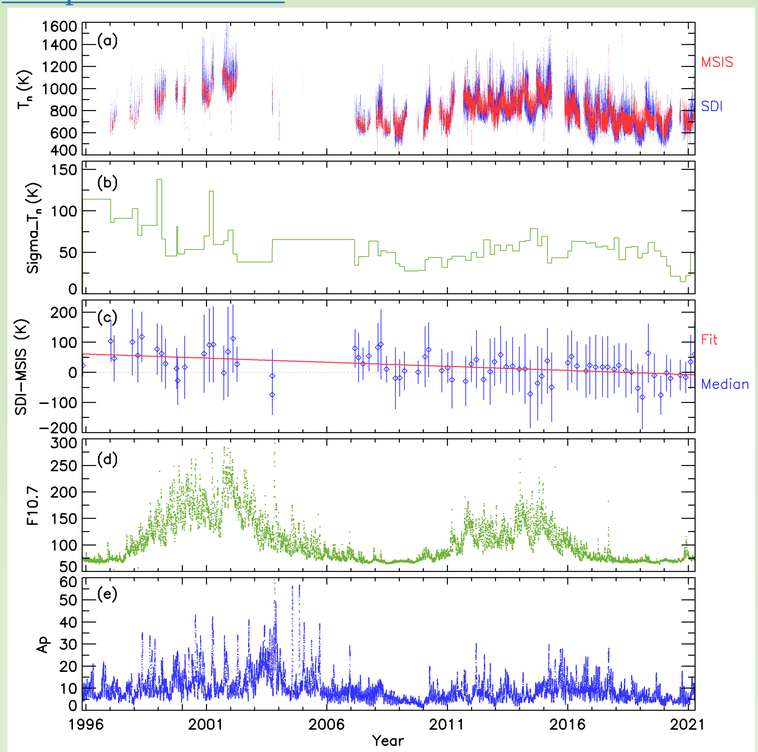

Figure 4. (a) Time series of SDI temperature and MSIS model temperature. **(b)** Median temperature uncertainties binned over 90 days period. **(c)** Blue diamonds show median (SDI minus MSIS) temperature differences, binned in 90-day intervals. The blue vertical bars at each time represent 1σ standard deviations of the temperature differences for each bin. The red solid line is a linear fit to the temperature differences and is showing the temperature trend over the period shown along the x-axis. **(d)** 10.7 cm solar radio flux in solar flux units. This panel shows that the SDI data cover more than two full solar cycles. **(e)** Geomagnetic Ap indices for the observation period.

The main points to be noted relating to Figure 4 are that:

1. The main cause of declining temperature uncertainty with time is the narrower passbands of newer instruments.
2. SDI minus MSIS model temperature differences were evaluated, and the results were binned into a 90-day period. A median value was determined for each bin. A linear fit to the resulting trimonthly medians shows a trend of -27.4±6.2 K/decade.
3. As there is no signature of F10.7 or Ap variation in the temperature trend, we infer that our results are not affected by F10.7 or Ap variation.

Conclusions:

1. **Our data show that the F-region neutral thermosphere around peak red-line emission altitude is cooling at the rate of -27.4±6.2 K/decade. Uncertainty in the trend is less than 25 % of the trend itself.**
2. Observed trend is significantly larger than that predicted by theory (Roble and Dickinson, 1989). However, the trend is comparable with previous results from studies of ISR data for ion temperatures.
3. Continuous monitoring of the neutrals in the upper atmosphere for an extended period is necessary for better trend accuracy and reliable prediction of possible changes in the upper atmosphere.

References:

1. Roble, R. G., & Dickinson, R. E. (1989). How will changes in carbon dioxide and methane modify the mean structure of the mesosphere and thermosphere?. *Geophysical Research Letters*, *16*(12), 1441-1444.
2. Conde, M., and Smith R. W., Mapping thermospheric winds in the Auroral zone, *Geophys. Res. Lett.*, 22, 3019-3022, 1995.
3. Conde, M., and Smith, R. W., Phase compensation of a separation scanned, all-sky imaging Fabry-Perot spectrometer for Auroral studies, *Appl. Opt.*, 36, 5441-5450, 1997.
4. Conde, M., and Smith, R. W., Spatial structure in the thermospheric horizontal wind above Poker Flat, Alaska, during solar minimum, *J. Geophys. Res.*, 103, 9449– 9471, 1998.
5. Conde, M., Bristow, W., Hampton, D., & Elliott, J. (2018). Multiinstrument studies of thermospheric weather above Alaska. Journal of Geophysical Research: Space Physics, 123 (11), 9836–9861.
6. Donaldson, J. K., Wellman, T. J., & Oliver, W. L. (2010). Long-term change in thermospheric temperature above Saint Santin. *Journal of Geophysical Research: Space Physics*, *115*(A11).
7. Zhang, S. R., Holt, J. M., & Kurdzo, J. (2011). Millstone Hill ISR observations of upper atmospheric long-term changes: Height dependency. *Journal of Geophysical Research: Space Physics*, *116*(A2).

Acknowledgement:

This work was supported by multiple NSF awards extending back to 1995.